Photorefractivity in liquid crystalline composite materials

Gary P. Wiederrecht[a] and Michael R. Wasielewski[a,b]

[a]Chemistry Division, Argonne National Laboratory, Argonne, IL 60439-4831
[b]Department of Chemistry, Northwestern University, Evanston, IL 60208-3113

ABSTRACT

We report recent improvements in the photorefractive performance of liquid crystalline thin film composites containing electron donor and acceptor molecules. The improvements primarily result from optimization of the exothermicity of the intermolecular charge transfer reaction and improvement of the diffusion characteristics of the photogenerated ions. Intramolecular charge transfer dopants produce greater photorefractivity and a 10-fold decrease in the concentration of absorbing chromophores. The mechanism for the generation of mobile ions is discussed.

Keywords: Photorefractive Materials; Semiconductor films; Non-Linear optics; Photoconductivity

1. INTRODUCTION

Liquid crystalline materials are of interest for a variety of applications in the areas of optical signal processing and photoinduced charge transport [1-4]. Recently, nematic liquid crystals have been utilized to produce photorefractive holograms [3,5-10]. The photorefractive effect holds great promise for reversible optical holography, noise-free optical image amplification, phase conjugate mirrors, and other optical signal processing techniques [11-16]. Photorefractivity is a light-induced change in the refractive index of a material. The mechanism for the refractive index change begins with a sample that weakly absorbs a laser beam. An appropriate sample will allow the absorbing chromophores to dissipate some of their energy through charge separation. Photovoltaic materials, or the application of an electric field, permit photoinduced directional charge transport over macroscopic distances. If the positive and negative charges have different mobilities, an electric field (or space charge field) is formed which modulates the index of refraction through either the linear or quadratic electrooptic effect. The maximization of the photorefractive effect is not an easy problem, because the electrooptic, charge generation, charge transport, and charge trapping characteristics of a material must be simultaneously optimized.

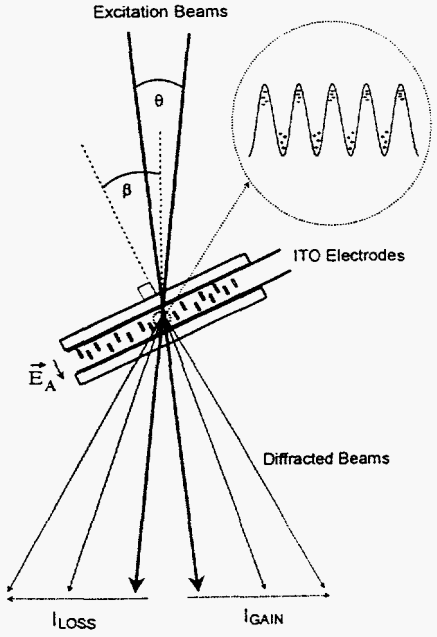

Figure 1

Nematic liquid crystals are novel photorefractive materials because their refractive index change is derived entirely from the quadratic electrooptic effect. Although this effect is usually associated with the high temperature centrosymmetric phase of inorganic ferroelectric crystals [17-19], the scope of this effect has become much broader with the recent advent of photorefractive polymers [20-24]. By decreasing the glass transition temperature of the host polymer, large increases in photorefractive gain are observed that can not be explained by the linear electrooptic effect [20,21]. The enhancement is due to an ordering of the birefringent NLO chromophores within the space-charge

DISCLAIMER

DISCLAIMER

Portions of this document may be illegible electronic image products. Images are produced from the best available original document.

field. For the most recent photorefractive polymers, the quadratic electrooptic (or orientational enhancement) effect has been shown to be responsible for a majority of the photorefractive gain [25]. One of the motivations for this work is that the orientational enhancement effect should be very large in liquid crystals due to their birefringent nature and the fact that they can reorient even within very small optical fields [6].

2. EXPERIMENTAL METHODS

In order to observe photorefractivity in nematic liquid crystals, they must first be doped with electron donors and/or acceptors that induce photoconductivity. This was initially accomplished by doping a nematic liquid crystal with dye molecules such as rhodamine 6G [5,6]. These dopants were limited by solubility and inefficient charge generation characteristics. We recently showed that by doping a eutectic mixture of nematic liquid crystals with electron donors and acceptors that have favorable redox properties, facile intermolecular charge transfer occurs, and a large photorefractive gain is observed [7-10]. The experimental configuration is shown in Figure 1 and utilizes two coherent beams from a continuous wave Ar^+ laser that are crossed in the sample. The beams are unfocused and have a $1/e$ diameter at the sample of 2.5 mm. Mixtures of 35% (weight %) 4'-(*n*-octyloxy)-4-cyanobiphenyl (8OCB) and 65% 5CB were homeotropically aligned on indium tin oxide (ITO) coated glass slides by treatment of the ITO with octadecyltrichlorosilane [26]. We found superior photorefractive effects in 8OCB/5CB relative to 5CB alone, presumably because of a greater reorientation angle of the 8OCB and 5CB molecules in the lower viscosity LC mixture [27]. The birefringence of 8OCB is also slightly greater than that of 5CB [28]. The samples vary in thickness between 12 and 100 μm, as determined by a Teflon spacer. Thinner samples permit higher electric fields to be applied because hydrodynamic turbulence resulting from charged particle motion between the two ITO plates is reduced [27]. A 1.5 V battery is utilized to apply electric fields of up to 0.4kV/cm to the sample.

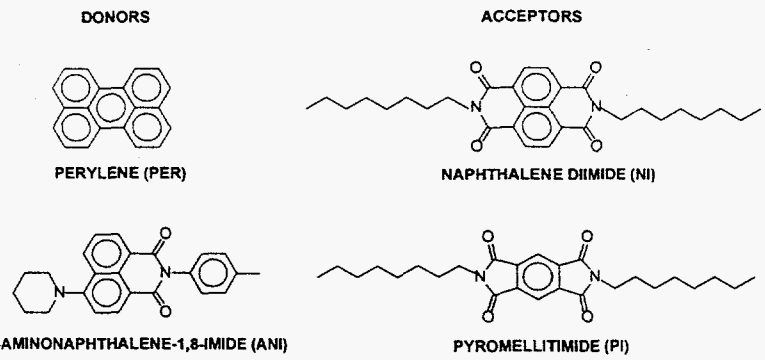

Figure 2. Intermolecular charge transfer dopants.

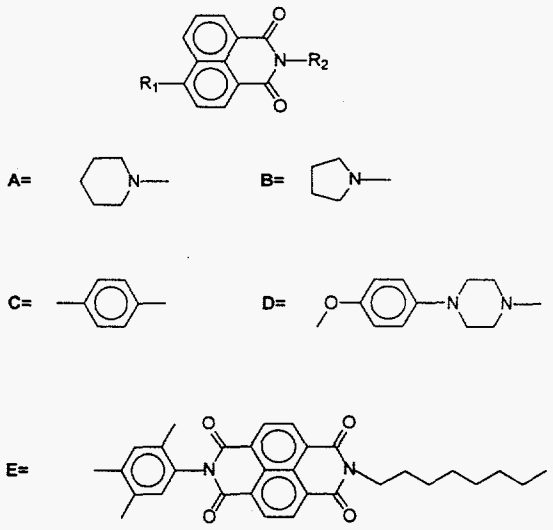

Compound	R_1	R_2
1	D	C
2	B	E
3	A	E
4	D	E
5	A	C

Figure 3. Intramolecular charge transfer dopants.

A variety intermolecular and intramolecular charge transfer dopants have been

utilized and are illustrated in Figures 2 and 3. They were chosen for the following reasons: (i) They are highly soluble in 8OCB/5CB; (ii) The donors have visible absorptions that extend to 514 nm, permitting all Ar^+ lines to be utilized, whereas the electron acceptors have no visible absorptions. Thus, the donor molecules serve as charge generators by absorbing light and transferring an electron to NI; (iii) The donors and acceptors are easily and reversibly oxidized and reduced, respectively, as illustrated in Table 1. The free energy for charge separation (ΔG_{CS}) was calculated using the relationship:

$$\Delta G_{CS} = E_{OX} - E_{RED} - \frac{e_o^2}{\varepsilon_s r_{12}} - E_s \qquad (1)$$

where E_{OX} is the oxidation potential of the donor, E_{RED} is the reduction potential of the acceptor, E_S is the first excited singlet state of the donor, e_o is the charge of an electron, ε_s is the static dielectric constant, and r_{12} is the center-to-center distance between the donor and acceptor. The coulomb attraction term containing the r_{12} value is not utilized for the intermolecular charge transfer dopants. Given these redox potentials, efficient charge generation in 8OCB/5CB can occur by excitation of the donor to its lowest excited singlet state (S_1), followed by electron transfer from S_1 to an acceptor, resulting in the production of cations and anions; (iv) The long axes of donors and acceptors align along the director of the liquid crystal, which enables the use of relatively high concentrations of dopants without destroying the LC phase of the 8OCB/5CB mixture.

Table 1. The lowest excited singlet state, redox potentials vs the saturated calomel electrode (SCE), and free energies for charge separation and return are given. The charge separation in **4** occurs in two steps. The first step is photoinduced with energetics that are the same as in **1**, while the second thermal electron transfer produces the final, more distant ion pair. Molecule **5** is a control molecule without an electron acceptor and therefore is not cited here.

Molecule	E_S (eV)	r_{12}	E_{OX} (V)	E_{RED} (V)	ΔG_{CS} (eV)	ΔG_{CR} (eV)
PER, NI	2.8	----	0.8	-0.5	-1.5	-1.3
PER, PI	2.8	----	0.8	-0.8	-1.2	-1.6
ANI, NI	2.8	----	1.0	-0.5	-1.3	-1.5
ANI, PI	2.8	----	1.0	-0.8	-1.0	-1.8
1	2.80	7.7	0.79	-1.41	-0.78	-2.02
2	2.48	15.2	1.08	-0.53	-0.96	-1.52
3	2.80	15.2	1.20	-0.53	-1.16	-1.64
4[a]	2.80	19.1	0.79	-1.41/-0.53	-0.78/-1.60	-1.17

3. INTERMOLECULAR CHARGE TRANSFER DOPANTS

An example of a two-beam coupling experiments utilizing a liquid crystal sample with a perylene concentration of 2.0×10^{-3} M and an NI concentration of 6.8×10^{-3} M in a 37-μm-thick sample is shown in Figure 4. The wave mixing angle was $\theta = 1.9 \times 10^{-3}$ rad. The total incident light intensity was only 100 mW/cm^2 (50 mW/cm^2 in each beam). At this intensity, five orders of diffraction were observed. For light intensities of 400 mW/cm^2, as many as eight orders were observed. Observation of two-beam coupling is the definitive criterion for the existence of a photorefractive grating in the thick grating regime [20]. Beam coupling due to photorefractivity has also been observed in the thin grating regime for semiconductor quantum wells, but the large optical absorption of these materials has precluded net photorefractive gain [16]. In addition, beam coupling has been observed in thin gratings as a consequence of thermal effects [29]. In the results presented here, the diffracted beams only appeared in the presence of an applied electric field, eliminating the possibility of beam coupling due to thermal gratings. In addition, the diffracted spots only appeared with extraordinary (p) polarized beams. In the multiple diffraction regime, beam coupling

manifested itself as an increase in the intensity of all of the diffracted and undiffracted light from one beam and a corresponding drop in the intensity of the other beam and its diffracted beams.

The photorefractive gain in these LC materials was measured in the following manner. I_1 is the intensity of beam 1 after the sample without beam 2 applied and I_{12} is the intensity of beam 1 after the sample with beam 2 applied. Correspondingly, I_2 is the intensity of beam 2 after the sample without beam 1 applied and I_{21} is the intensity of beam 2 with beam 1 applied. In the thin grating regime the value of I_1 must be corrected because much of the energy in beam 1 is diffracted into higher order beams. Following this correction [30], the data yield a beam coupling ratio I_{12}/I_1 as high as 1.88. Similar measurements for beam 2, corrected for diffraction, give a beam coupling ratio I_{21}/I_2 as low as 0.11. Thus, the data are in good agreement, indicating that one beam gains 88% of its intensity, whereas the other loses 89% of its intensity. At these values, the grating fringe spacing (Λ) equals 57 μm and the grating has a $1/e$ rise time of 14 s.

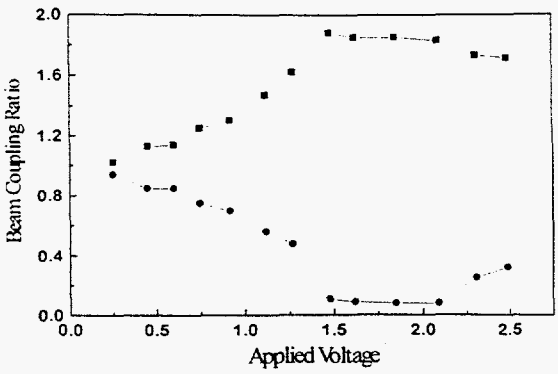

Figure 4. A plot of beam coupling ratio versus applied voltage is shown for both the beam that gains intensity (■) and for the beam that loses intensity (●).

In order to more fully understand the mechanism for charge generation in liquid crystals, a more detailed study of the magnitude of the photorefractive effect as a function of the driving force for charge generation was performed. The results of this study can be better understood through the equation for a modulated space-charge field formed by diffusing ions [3,6]:

$$E_{sc} = \frac{-k_B T q}{2e_o} \frac{D^+ - D^-}{D^+ + D^-} \frac{\sigma_{ph}}{\sigma_{ph} + \sigma_d} \sin qx \qquad (2)$$

Here, σ_{ph} is the photoconductivity, σ_d is the dark conductivity, k_B is the Boltzmann constant, e_o is the charge of a proton, q is the wavevector of the grating, and D^+ and D^- are the diffusion constants for the cations and anions, respectively. It is clear that the two factors which determine the magnitude of the space charge field are the difference in the photoconductivity versus dark conductivity and the difference in the diffusion coefficients of the cations and anions. These factors allow for one set of charges to remain in the illuminated regions of the interference pattern and for the opposing charges to migrate into the nulls of the interference pattern.

Further quantitation can be experimentally determined through the relation of these quantities to the diffraction efficiency η of a Raman-Nath orientational grating: [6,31]

$$\eta = \left(\frac{Lmk_b T}{\lambda_{opt} n_e K q e_o} \frac{E_A \varepsilon_s \varepsilon_\infty \sin\beta}{1 + \frac{\varepsilon_s E_A}{2\pi K q^2}} \nu \frac{\sigma_{ph}}{\sigma_{ph} + \sigma_d} \right)^2 \qquad (3)$$

where

$$\nu = \frac{D^+ - D^-}{D^+ + D^-} \qquad (4)$$

where L is the thickness of the sample, n_e is the index of refraction along the extraordinary axis, K is the single constant approximation of the Frank elastic constant, E_a is the applied electric field, ε_s is the static dielectric constant, λ_{opt} is the laser wavelength, and ε_∞ is the high frequency dielectric constant. Fortunately, the only variables that are a function of the dopants are the diffusion and conductivity terms. Rudenko and Sukhov showed that the conductivity term in Eq. 3 saturates at higher light intensities, permitting ν to be determined.

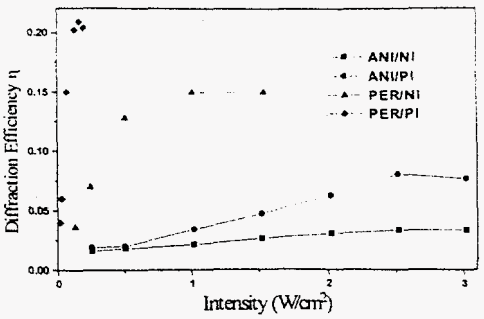

Figure 5. The saturation diffraction efficiencies for four liquid crystal composites are shown.

The results of this study with the intermolecular donors and acceptors are shown in Figure 5. The parameters determined from the diffraction efficiency measurements are given in Table 2. Time of flight measurements were performed to determine the diffusion coefficients for D^- of NI^- and D^+ of ANI^+, which can be utilized in conjunction with Eq. 4 to determine the remaining diffusion coefficients. The data indicate that there is a large difference in the values of ν. For the ANI/NI system, the time of flight measurements show that the anion (NI^-) is more mobile than the cation (ANI^+). The results shown in Fig. 5 further support this conclusion, since the values for ν are larger for the PI acceptors for a given donor chromophore. Since PI is smaller, it stands to reason that its increased mobility will produce a larger value for ν than NI doped samples. It follows from Fig. 3 that PER is less mobile than ANI chromophores, because samples doped with PER have superior saturation diffraction efficiencies for a given acceptor. Thus, the best sample is the PER/PI combination which has a value for ν of 0.21, more than 10 times better than the R6G/5CB samples.

A particularly intriguing aspect of the data, however, is that the PER/PI sample saturates at much lower intensities (100 mW/cm^2) than the other composites. This can only mean that the efficiency of mobile charge generation is much greater in this sample. At first glance, this seems counterintuitive since the more easily reduced NI sample would suggest a better charge separation efficiency. However, Marcus theory predicts that the rate of charge separation (k_{CS}) will be the greatest when the exothermicity of the reaction is equal to the sum of the reorganization energy of the solvent (λ_o) and the internal vibrational reorganization energy of the ions (λ_i) [32-34]. For free energies of charge separation that are more or less than the total reorganization energy, the rates of charge separation will be slower. This can be restated by the equations: [32-34]

$$k_{CS} = \left(\frac{2\pi}{\hbar}\right) V_{DA}^2 \left(\frac{1}{4\pi\lambda RT}\right)^{1/2} \exp\left(-E_a / RT\right) \tag{5}$$

where

$$E_a = \frac{\left(\Delta G_{CS} + \lambda\right)^2}{4\lambda} \tag{6}$$

$$\lambda = \lambda_0 + \lambda_i . \tag{7}$$

Here, V_{DA} is the electronic coupling matrix element between the donor and acceptor. From the data, it appears that the rate for charge separation is maximized for the PER/PI system in which ΔG_{CS} is -1.2 eV. Following previous precedent, these values ignore the Coulomb term which is small in polar environments[34]. Although the optimal ΔG_{CS} value at first glance appears to be rather high, it has been established that the solvent reorganization energies for solvent separated ion pairs, as opposed to tight ion pairs, are higher[34].

In addition to optimizing ΔG_{CS}, the free energy for charge return in the PER/PI system is greater than that for PER/NI. This places ΔG_{CR} farther out in the Marcus inverted regime for the PER/PI system, resulting in slower rates for charge return and therefore increasing the efficiency of mobile charge

generation [34]. Thus, the PER/PI liquid crystal composite appears to be the best of both worlds: it has the largest value for ν, which maximizes E_{SC}, and also has the best efficiency of mobile charge generation.

Table 2. The saturation diffraction efficiencies (η_{SAT}), wavevectors (q), ν, and diffusion coefficients for each molecular component are given.

Molecule	η_{SAT}	q x 10^{-3} cm^{-1}	ν	D^+ x 10^8 cm^2/sec	D^- x 10^8 cm^2/sec
PER, NI	0.15	4.7	0.17	2.5	3.4
PER, PI	0.21	4.7	0.21	2.5	3.8
ANI, NI	0.033	4.2	0.11	2.7	3.4
ANI, PI	0.080	4.2	0.17	2.7	3.8

4. INTRAMOLECULAR CHARGE TRANSFER DOPANTS

A limitation of the above composites is that the charge generation efficiency is limited by the excited state lifetime of the absorbing electron-donating chromophore. It must collide with an electron acceptor during its lifetime or no charge generation will occur. However, it is known that the lifetimes of intramolecular ion pairs are increased by a thousand times or more in liquid crystals [35]. We now report photorefractivity in liquid crystals that are doped with electron donor-acceptor molecules that undergo efficient photoinduced *intramolecular* charge separation. Since the observation of photorefractivity in liquid crystals relies on migration of charges over several microns, we show that the initial intramolecular charge separation is followed by intermolecular charge separation that results in bulk charge migration. The magnitude of the observed photorefractivity is found to be a function of the lifetime of the intramolecular charge separated state. We further show that intramolecular charge transfer dopants provide a more efficient mechanism for producing photorefractivity than intermolecular charge transfer dopants. This permits lower dopant concentrations, that in turn reduce absorption losses in these materials.

For quantitative comparison of the grating strengths in the different liquid crystal composites, the first order diffraction efficiency measurements of the Raman-Nath gratings are reported. Several concentrations for each of the dopants were utilized and Figure 6 illustrates the highest diffraction efficiency values vs. applied voltage for the samples with the optimal concentration of each dopant. A wavevector value of q = $1.1x10^3$ cm^{-1} was again utilized. The first clearly noticeable fact is that the intramolecular charge transfer molecules **3** and **4** are superior to the intermolecular charge transfer dopants for inducing photorefractivity. For these dopants, larger diffraction efficiencies are achieved at lower applied fields. Photorefractivity for **3** is observed for an applied voltage as low as 0.2 V, corresponding to an applied field of only 50 V/cm. For applications purposes, **3** has superior chemical stability in the liquid crystals relative to **4**. Apparently, the methoxy group of **4** leads to photoinstability in the 5CB/8OCB environment, which leads to a loss of photorefractivity over a few days. The voltages were not increased to higher values for these samples because the measurements were not found to be reliable for very strong gratings with numerous (>5) diffracted beams. Also, theories relating the diffraction efficiency of Raman-Nath gratings to various physical

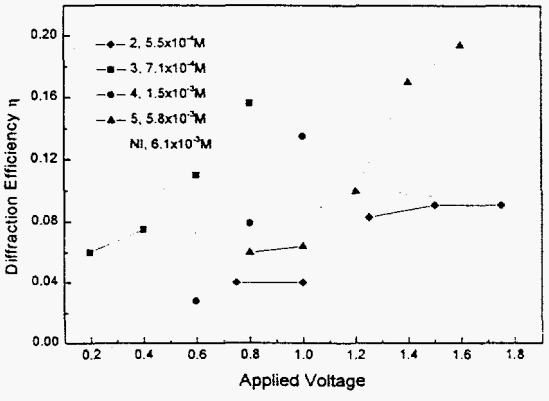

Figure 6 The diffraction efficiency of the photorefractive grating in the composite systems is illustrated. Note that high diffraction efficiency for the composites containing the intramolecular charge transfer dopants occurs at lower applied voltages than those for the intermolecular charge transfer dopants.

parameters are not valid for diffraction efficiencies above approximately 0.2.

The magnitude of the diffraction efficiency for samples with intramolecular dopants **1-4** is clearly dependent upon the lifetime of the charge separated state. Dopant **1** has no measurable photorefractivity and a charge separated lifetime of only 530 ns in the liquid crystal. Dopant **2** has a charge separated lifetime of 770 ns and has diffraction efficiency comparable to that for samples doped with **5**. Liquid crystal composites containing dopants **3** and **4**, that have ion pair lifetimes of 4.4 and 3.2 ms, respectively, have dramatically increased photorefractivity over composites that contain dopants with shorter ion pair lifetimes.

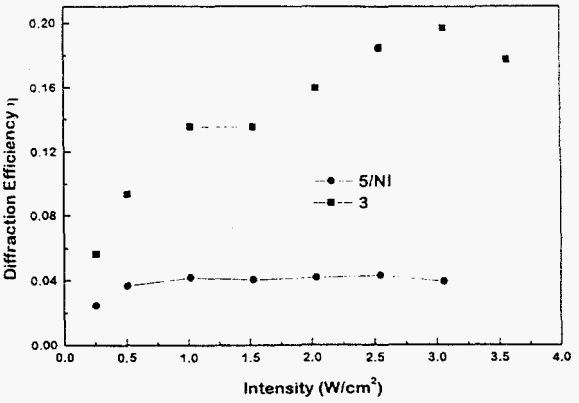

Figure 7 The diffraction efficiency of the photorefractive grating as a function of optical intensity is shown for composites containing either 3 or 5/NI. The 5/NI sample saturates at lower intensities than the composite containing 3. The grating spacing is 16.9 μm.

The dependence of diffraction efficiency on the dopants' ion pair lifetime points to charge hopping as a mechanism for charge transport, because the likelihood that charges will hop to neighboring molecules increases with the lifetime of the charge separated state. Schemes 1 and 2 indicate the proposed mechanisms for bulk charge separation for composites containing intermolecular and intramolecular charge transfer dopants, respectively. Charge hopping in liquids has long been discussed as an enhancement mechanism for conduction in addition to diffusion. For example, electron-exchange mechanisms were first discussed by Levich and Dahms [36,37]. Ruff and Friedrich generalized these theories and named the process "transfer diffusion" [38]. This process has also been discussed in the framework of Marcus theory [39].

Figure 7 illustrates a plot of η as function of intensity for samples with dopant **3** (7.1×10^{-4}M) and **5/NI** (both have concentrations of 5.8×10^{-3}M). The values of η in the saturation limit are different by a factor of five, indicating that ν much larger for the sample doped with **3** relative to that doped with **5/NI.** We obtain values for $\nu = 0.29$ for the composite containing **3** and $\nu = 0.04$ for the samples containing **5/NI**. Thus, the values for ν show conclusively that the difference in the diffusion coefficients is much larger for the intramolecular charge transfer dopants relative to the intermolecular charge transfer dopants.

5. CONCLUSIONS

We have induced large photorefractive grating diffraction efficiencies in nematic liquid crystals by doping them with molecules that undergo intermolecular and intramolecular charge separation. Although both types of charge generators produce excellent photorefractivity, the intramolecular charge transfer dopants are shown to be superior for inducing photorefractivity relative to identical electron donors and acceptors which must undergo intermolecular charge separation. This is shown to be a result of several factors. The first is the larger difference between the magnitude of the diffusion coefficients of the cation and anion for the intramolecular charge transfer dopants relative to the intermolecular dopants. It is also shown that the magnitude of the photorefractive effect increases with longer ion pair lifetimes for the intramolecular charge transfer dopants. This is consistent with Marcus theory and transfer diffusion theory, which describes bulk charge migration through charge hopping between donor-acceptor molecules. The greater efficiency of mobile charge generation for the intramolecular charge transfer dopants permits the use of lower concentrations and reduced absorption of the samples.

Acknowledgments

We gratefully acknowledge support from the Office of Computational and Technology Research, Division of Advanced Energy Projects and Technology Research, U.S. Department of Energy, under contract W-31-109-ENG-38.

References

1. Adam, D.; Schuhmacher, P.; Simmerer, J.; Haussling, L.; Siemensmeyer, K.; Etzbach, K. H.; Ringsdorf, H.; Haarer, D. *Nature* **371**, pp. 141-143, 1994.
2. Gregg, B. A.; Fox, M. A.; Bard, A. J. *J. Phys. Chem.* **94**, pp. 1586-1598, 1990.
3. Khoo, I. C. *Opt. Lett.* **20**, pp. 2137-2139, 1995.
4. Schouten, P. G.; Warman, J. M.; Haas, M. P. d.; Fox, M. A.; Pan, H. L. *Nature* **353**, pp. 736, 1991.
5. Khoo, I. C.; Li, H.; Liang, Y. *Opt. Lett.* **19**, pp. 1723-1725, 1994.
6. Rudenko, E. V.; Sukhov, A. V. *JETP Lett.* **59**, pp. 142-145, 1994.
7. Wiederrecht, G. P.; Yoon, B. A.; Wasielewski, M. R. *Science* **270**, pp. 1794-1797, 1995.
8. Wiederrecht, G. P.; Yoon, B. A.; Wasielewski, M. R. *Adv. Mat.* **8**, pp. 535-539, 1996.
9. Wiederrecht, G. P.; Yoon, B. A.; Wasielewski, M. R. *Synth. Met.* **84**, pp. 901-902, 1997.
10. Wiederrecht, G. P.; Yoon, B. A.; Svec, W. A.; Wasielewski, M. R. *J. Am. Chem. Soc.* **119**, pp. 3358-3364, 1997.
11. Gunter, P.; Huignard, J. P. *Photorefractive Materials and Their Applications 1: Fundamental Phenomena*; Springer-Verlag: Berlin, 1988.
12. Feinberg, J.; Hellwarth, R. W. *Opt. Lett.* **5**, pp. 519-521, 1980.
13. Feinberg, J. *Physics Today* **October**, pp. 46-52, 1988.
14. White, J. O.; Yariv, A. *Appl. Phys. Lett.* **37**, pp. 5-7, 1980.
15. Anderson, D. Z.; Lininger, D. M.; Feinberg, J. *Opt. Lett.* **12**, pp. 123-125, 1987.
16. Nolte, D. D.; Olson, D. H.; Doran, G. E.; Knox, W. W.; Glass, A. M. *J. Opt. Soc. Am. B* 7, pp. 2217-2225, 1990.
17. Orlowski, R.; Boatner, L. A.; Kratzig, E. *Opt. Commun.* **35**, pp. 45-48, 1980.
18. Chen, F. S. *J. Appl. Phys.* **38**, pp. 3418-3420, 1967.
19. von der Linde, D.; Glass, A. M.; Rodgers, K. F. *Appl. Phys. Lett.* **26**, pp. 155-157, 1975.
20. Moerner, W. E.; Silence, S. M. *Chem. Rev.* **94**, pp.127-155, 1994.
21. Meerholz, K.; Volodin, B. L.; Sandalphon; Kippelen, B.; Peyghambarian, N. *Nature* **371**, pp. 497-500, 1994.
22. Liphardt, M.; Goonesekera, A.; Jones, B. E.; Ducharme, S.; Takacs, J. M.; Zhang, L. *Science* **263**, pp. 367-369, 1994.
23. Zhang, Y.; Cui, Y.; Prasad, P. N. *Phys. Rev. B* **46**, pp. 9900-9902, 1992.
24. Yu, L.; Chan, W. K.; Peng, A.; Gharavi, A. *Acc. Chem. Res.* **29**, pp. 13, 1996.
25. Meerholz, K.; Kippelen, B.; Peygambarian, N. *The Spectrum* **8**, pp. 1-7, 1995.
26. Khoo, I. C. *Liquid Crystals: Physical Properties and Nonlinear Optical Phenomena*; Wiley: New York, 1995.
27. Collings, P. J. *Liquid Crystals: Nature's Delicate Phase of Matter*; Princeton Univ. Press: Princeton, 1990.
28. Sen, S.; Brahma, P.; Roy, S. K.; Mukherjee, D. K.; Roy, S. B. *Mol Cryst. Liq. Cryst.* **100**, pp. 327-340, 1983.
29. Yan, P. Y.; Khoo, I. C. *IEEE J. Quant. Elec.* **25**, pp. 520-534, 1989.
30. The value for I_1 in this experiment is given by the relation $I_1=I_o(1-\eta T)$, where I_0 is the intensity in beam 1 after the sample in the absence of diffraction and η_T is the total diffraction efficiency of the grating. For the case of an applied electric field of 0.4 kV/cm, the value for I_1 was 68% (34 mW/cm^2) of the value of I_0 without the electric field. In other words, 32% of the total power lies in the diffracted spots. It is reasonable to consider the 34 mW/cm^2 as the correct value of I_1 for the beam coupling calculations. Subsequently, with both beams incident on the sample, beam 1 was found to increase in intensity to 64 mW/cm^2.
31. Tabiryan, N. V.; Sukhov, A. V.; Zeldovich, b. Y. *Mol. Cryst. Liq. Cryst.* **135**, pp. 1-139, 1986.
32. Wasielewski, M. R. *Chem. Rev.* **92**, pp. 435-461, 1992.
33. Marcus, R. A. *J. Chem. Phys.* **24**, pp. 966-978, 1956.

34. Gould, I. R.; Ege, D.; Moser, J. E.; Farid, S. *J. Am. Chem. Soc.* **112**, pp. 4290-4301, 1990.
35. Hasharoni, K.; Levanon, H.; Greenfield, S. R.; Gosztola, D. J.; Svec, W. A.; Wasielewski, M. R. *J. Am. Chem. Soc.* **118**, pp. 10228-10235, 1996.
36. Dahms, H. *J. Phys. Chem.* **72**, pp. 362-364, 1968.
37. Levich, V. G. *Adv. Electrochem. Eng.* **4**, pp. 314-316, 1966.
38. Ruff, I.; Friedrich, V. J. *J. Phys. Chem* **75**, pp. 3297-3302, 1971.
39. Suga, K.; Aoyagui, S. *Bull. Chem. Soc. Jpn.* **46**, pp. 755-761, 1973.